PRAMANA
— journal of
physics

Vol. 67, No. 6
December 2006
pp. 1129–1140

Mode-to-mode energy transfers in convective patterns

MAHENDRA K VERMA[1], KRISHNA KUMAR[2] and BHASKAR KAMBLE[1]
[1]Department of Physics, Indian Institute of Technology Kanpur, Kanpur 208 016, India
[2]Department of Physics, Indian Institute of Technology Kharagapur, Kharagpur 721 302, India
E-mail: mkv@iitk.ac.in

MS received 8 May 2006; accepted 22 August 2006

Abstract. We investigate the energy transfer between various Fourier modes in a low-dimensional model for thermal convection. We have used the formalism of *mode-to-mode energy transfer rate* in our calculation. The evolution equations derived using this scheme is the same as those derived using the hydrodynamical equations for thermal convection in Boussinesq fluids. Numerical and analytical studies of this model show that convective rolls appear as the Rayleigh number R is raised above its critical value R_c. Further increase of Rayleigh number generates rolls in the perpendicular directions as well, and we obtain a dynamic asymmetric square pattern. This pattern is due to Hopf bifurcation. There are two sets of limit cycles corresponding to the two competing asymmetric square patterns. When the Rayleigh number is increased further, the limit cycles become unstable simultaneously, and chaotic motion sets in. The onset of chaos is via intermittent route. The trajectories wander for quite a long time almost periodically before jumping irregularly to one of the two *ghost* limit cycles.

Keywords. Convection; patterns.

PACS Nos 47.20.Ky; 47.27.-i; 47.27.E–

1. Introduction

Modal energy transfer [1–9] in fluids governs the nature of dynamics among small or large scale structures in fluids. The interactions of various possible structures and the resulting dynamics are controlled by the mechanism of energy transfer among these structures. In the case of cellular instability in fluids, more than one structure may be possible. The competition among these patterns involves exchange of energy between various structures. Many of the interesting dissipative structures in fluid either at primary or secondary instability involve triad interaction among critical modes and modes generated due to nonlinearity. We apply this idea to investigate mode-to-mode energy transfer in competing convective structures in a model of thermal convection at the onset of secondary instability. We also study

the possibility of chaos in the model of competing rolls and asymmetric square structures. The chaos sets in through intermittency.

2. Hydrodynamical equations

The hydrodynamics of thermal convection in a thin layer of thickness d of a Boussinesq fluid confined between two conducting horizontal plates, and subjected to adverse temperature gradient β is governed by

$$\frac{\partial \mathbf{u}}{\partial t} + (\mathbf{u}\cdot\nabla)\mathbf{u} = -\frac{1}{\rho}\nabla\sigma + g\alpha\theta\hat{\mathbf{z}} + \nu\nabla^2\mathbf{u}, \tag{1}$$

$$\frac{\partial \theta}{\partial t} + (\mathbf{u}\cdot\nabla)\theta = \beta\mathbf{u}\cdot\hat{\mathbf{z}} + \kappa\nabla^2\theta, \tag{2}$$

$$\nabla\cdot\mathbf{u} = 0, \tag{3}$$

where $\mathbf{u}$ is the velocity field, θ and σ are the deviations in the temperature and pressure fields from their values in the conduction state. The thermal expansion coefficient α, the kinematic viscosity ν, the thermal diffusivity κ, and a reference density ρ are assumed to have uniform values in the fluid, which is compatible with Boussinesq approximation. The conducting plate requires the deviations in the temperature field to vanish ($\theta = 0$) at the horizontal plates. We assume the plates to be stress-free, which is an idealized condition on velocity fields. This assumption requires the vertical velocity (u_3) and the vertical gradients of horizontal velocities to vanish ($\partial_z u_1 = \partial_z u_2 = 0$) at the bounding surfaces.

The nondimensionalization of all length scales by the fluid depth d, time scales by the thermal diffusive time d^2/κ, and the temperature field by the temperature difference βd across the fluid, yield the following nondimensional equations:

$$\frac{\partial \mathbf{u}}{\partial t} + (\mathbf{u}\cdot\nabla)\mathbf{u} = -\nabla\sigma + RP\theta\hat{\mathbf{z}} + P\nabla^2\mathbf{u},$$
$$\frac{\partial \theta}{\partial t} + \mathbf{u}\cdot\nabla)\theta = u_3 + \nabla^2\theta,$$

where the nondimensional parameters $R = \alpha g\beta d^4/\nu\kappa$ and $P = \nu/\kappa$ are Rayleigh and Prandtl numbers respectively. The form of continuity equation remains the same in the dimensionless form.

3. Model and formalism of mode-to-mode energy transfer

Writing the above hydrodynamical equations in Fourier space, we get

$$\frac{\partial u_i(\mathbf{k})}{\partial t} = -ik_i\sigma(k) - ik_j \sum_{\mathbf{p}+\mathbf{q}=\mathbf{k}} u_j(\mathbf{q})u_i(\mathbf{p}) + RP\theta(\mathbf{k})\delta_{i3} - k^2 u_i(\mathbf{k}), \tag{4}$$

$$\frac{\partial\theta(\mathbf{k})}{\partial t} = u_3(k) - ik_j \sum_{\mathbf{p}+\mathbf{q}=\mathbf{k}} u_j(\mathbf{q})\theta(\mathbf{p}) - k^2\theta(\mathbf{k}),$$
$$k_i u_i(\mathbf{k}) = 0, \tag{5}$$

where $\mathbf{k} = \mathbf{p} + \mathbf{q}$. We can derive interesting results by focussing on a single triad $(\mathbf{k}', \mathbf{p}, \mathbf{q})$ such that $\mathbf{k}' + \mathbf{p} + \mathbf{q} = 0$. Clearly $\mathbf{k}' = -\mathbf{k}$. This is equivalent to truncating the expansion of the field to a single triad. We can easily derive the following energy equations:

$$\frac{\partial}{\partial t}\frac{|\mathbf{u}(\mathbf{k}')|^2}{2} = S^{uu}(\mathbf{k}'|\mathbf{p}|\mathbf{q}) + S^{uu}(\mathbf{k}'|\mathbf{q}|\mathbf{p}) + RP\Re\left[\theta(\mathbf{k})u_3^*(\mathbf{k})\right] - 2\nu k^2\frac{|\mathbf{u}(\mathbf{k}')|^2}{2}, \tag{6}$$

$$\frac{\partial}{\partial t}\frac{|\theta(\mathbf{k}')|^2}{2} = S^{\theta\theta}(\mathbf{k}'|\mathbf{p}|\mathbf{q}) + S^{\theta\theta}(\mathbf{k}'|\mathbf{p}|\mathbf{q}) + \Re\left[\theta(\mathbf{k})u_3^*(\mathbf{k})\right] - 2\kappa k^2\frac{|\theta(\mathbf{k}')|^2}{2}, \tag{7}$$

where

$$S^{uu}(\mathbf{k}'|\mathbf{p}|\mathbf{q}) = -\Im\left([\mathbf{k}'\cdot\mathbf{u}(\mathbf{q})]\,[\mathbf{u}(\mathbf{k}')\cdot\mathbf{u}(\mathbf{p})]\right), \tag{8}$$
$$S^{\theta\theta}(\mathbf{k}'|\mathbf{p}|\mathbf{q}) = -\Im\left([\mathbf{k}'\cdot\mathbf{u}(\mathbf{q})]\,[\theta(\mathbf{k}')\cdot\theta(\mathbf{p})]\right). \tag{9}$$

Here $\Re$ and $\Im$ represent the real and imaginary part of the argument. The quantity $S^{uu}(\mathbf{k}'|\mathbf{p}|\mathbf{q})$ $[S^{\theta\theta}(\mathbf{k}'|\mathbf{p}|\mathbf{q})]$ represents the energy transfer from the mode $\mathbf{u}(\mathbf{p})$ $[\theta(\mathbf{p})]$ (the field variable with the second argument) to the mode $\mathbf{u}(\mathbf{k}')$ $[\theta(\mathbf{k}')]$ (the field variable with the first argument) with the help of the mode $\mathbf{u}(\mathbf{q})$ $[\theta(\mathbf{q})]$ (the field variable with the third argument) acting as a mediator. The above formalism is called '*mode-to-mode*' formalism for energy transfer [2,9], and it differs from Kraichnan's '*combined energy transfer*' formalism [6,7]. For details refer to Dar *et al* [2] and the review paper by Verma [9]. The energy equation can be interpreted as follows: The field variables with wave number $\mathbf{k}'$ $[\mathbf{u}(\mathbf{k}'), \theta(\mathbf{k}')]$ receives energy from the modes $\mathbf{p}$ and $\mathbf{q}$ through mode-to-mode energy transfer terms, and it also receives energy from the interaction term $\theta(\mathbf{k})u_3^*(\mathbf{k})$.

It is important to keep in mind that $|\theta(\mathbf{k})|^2/2$ is not real energy. However, it has structure of energy, and we can apply the energy transfer formalism here as well. This idea has been exploited heavily in the past to infer the direction of flux of passive scalar etc. [5]. Dar *et al* [2] and Verma [9] have shown that the sum of all energy transfer rates along u–u and θ–θ channels are zero, i.e.,

$$S^{XX}(\mathbf{k}'|\mathbf{p}|\mathbf{q}) + S^{XX}(\mathbf{k}'|\mathbf{q}|\mathbf{p}) + S^{XX}(\mathbf{p}|\mathbf{k}'|\mathbf{q}) + S^{XX}(\mathbf{p}|\mathbf{q}|\mathbf{k}') + S^{XX}(\mathbf{q}|\mathbf{k}'|\mathbf{p}) + S^{XX}(\mathbf{q}|\mathbf{p}|\mathbf{k}') = 0,$$

where XX could be uu or $\theta\theta$.

Using this identity we can easily show that in the absence of viscous and thermal diffusivity

$$\frac{\partial}{\partial t}[|\mathbf{u}(\mathbf{k}')|^2+|\mathbf{u}(\mathbf{p})|^2+|\mathbf{u}(\mathbf{q})|^2] = 2RP\Re[\theta(\mathbf{k}')u_3^*(\mathbf{k}') + \theta(\mathbf{p})u_3^*(\mathbf{p})] + \theta(\mathbf{q})u_3^*(\mathbf{q})],$$

and

$$\frac{\partial}{\partial t}[|\theta(\mathbf{k}')|^2+|\theta(\mathbf{p})|^2+|\theta(\mathbf{q})|^2] = \Re[\theta(\mathbf{k}')u_3^*(\mathbf{k}') + \theta(\mathbf{p})u_3^*(\mathbf{p})] + \theta(\mathbf{q})u_3^*(\mathbf{q})].$$

The interpretation of the above equations is that the triad $[\mathbf{u}(\mathbf{k}'),\mathbf{u}(\mathbf{p}),\mathbf{u}(\mathbf{q})]$ and the triad $[\theta(\mathbf{k}'),\theta(\mathbf{p}),\theta(\mathbf{q})]$ exchange energy between each other via $\theta(\mathbf{k})u_3^*(\mathbf{k})$ interaction terms. The mode-to-mode interaction $S^{XX}(\mathbf{k}'|\mathbf{p}|\mathbf{q})$ conserves energy within a triad. The viscous and diffusive terms dissipate kinetic energy and θ energy respectively.

Equations (1)–(3) support heat flow through conduction (no motion) below critical Rayleigh number R_c. Just above R_c, convection sets in. For Boussinesq fluids confined between conductive plates, the convection appear in the form of stationary two-dimensional (2D) rolls at the onset of the convection. At higher Rayleigh number, this structure becomes unstable and new structures appear. We consider the model of Das *et al* [10], which allows competition between two mutually perpendicular sets of rolls. This study explores the possibility of convective cells in the form of asymmetric squares. Convective square structures are studied in pure fluids [11] as well as in binary mixtures [12,13]. Since the hydrodynamical equations for the thermal convection has two quadratic non-linearities, modes with higher wave numbers are generated that interact with each other and with the critical modes. These triadic interactions generate convective structures, which have been studied widely (for instance, see [14,15]). In the present paper, we study the interacting convective rolls using the mode-to-mode energy transfer formalism. Following Das *et al* [10] we consider the following truncated mode expansion of the relevant fields:

$$\begin{aligned}
u_1 &= -\frac{\pi}{k}w_{101}\sin kx\cos\pi z - \frac{\pi}{k}w_{112}\sin kx\cos ky\cos 2\pi z,\\
u_2 &= -\frac{\pi}{k}w_{011}\sin ky\cos\pi z - \frac{\pi}{k}w_{112}\cos kx\sin ky\cos 2\pi z,\\
u_3 &= [w_{101}\cos kx + w_{011}\cos ky]\sin\pi z\\
&\quad + w_{112}\cos kx\cos ky\cos 2\pi z,\\
\theta &= [\theta_{101}\cos kx + \theta_{011}\cos ky]\sin\pi z\\
&\quad + \theta_{112}\cos kx\cos ky\sin 2\pi z + \theta_{002}\sin 2\pi z.
\end{aligned}$$

The selection of these modes were motivated to investigate the possibility of symmetric and asymmetric squares cellular structures in convecting fluids following the experimental observations of Assenheimer and Steinberg [16] and numerical observations of Busse and Clever [11] (also refer to Sanchez-Alvarez *et al* [17]). An inspection of the chosen fields indicates that we have the following six sets of triads:

Mode	I	II	III	IV	V	VI
$\mathbf{k}'$	(1,0,1)	(1,0,1)	(−1,0,1)	(−1,0,1)	(1,0,1)	(0,1,1)
$\mathbf{p}$	(0,1,1)	(0,−1,1)	(0,1,1)	(0,−1,1)	(−1,0,1)	(0,−1,1)
$\mathbf{q}$	(−1,−1,−2)	(−1,1,−2)	(1,−1,−2)	(1,1,−2)	(0,0,−2)	(0,0,−2)

The numbers in the brackets represent the components along the x, y and z directions. The amplitudes of fields are given below:

Modes	u_1	u_2	u_3	θ
(1,0,1)	$-\frac{\pi}{4ki}w_{101}$	0	$\frac{1}{4i}w_{101}$	$\frac{1}{4i}\theta_{101}$
(−1,0,1)	$\frac{\pi}{4ki}w_{101}$	0	$\frac{1}{4i}w_{101}$	$\frac{1}{4i}\theta_{101}$
(0,1,1)	0	$-\frac{\pi}{4ki}w_{011}$	$\frac{1}{4i}w_{011}$	$\frac{1}{4i}\theta_{011}$
(0,−1,1)	0	$\frac{\pi}{4ki}w_{011}$	$\frac{1}{4i}w_{011}$	$\frac{1}{4i}\theta_{011}$
(−1,−1,−2)	$\frac{\pi}{8ki}w_{112}$	$\frac{\pi}{8ki}w_{112}$	$-\frac{1}{8i}w_{112}$	$-\frac{1}{8i}\theta_{112}$
(−1,1,−2)	$\frac{\pi}{8ki}w_{112}$	$-\frac{\pi}{8ki}w_{112}$	$-\frac{1}{8i}w_{112}$	$-\frac{1}{8i}\theta_{112}$
(1,−1,−2)	$-\frac{\pi}{8ki}w_{112}$	$\frac{\pi}{8ki}w_{112}$	$-\frac{1}{8i}w_{112}$	$-\frac{1}{8i}\theta_{112}$
(1,1,−2)	$-\frac{\pi}{8ki}w_{112}$	$-\frac{\pi}{8ki}w_{112}$	$-\frac{1}{8i}w_{112}$	$-\frac{1}{8i}\theta_{112}$
(0,0,−2)	0	0	0	$-\frac{1}{2i}\theta_{002}$

Using eq. (7) we write the equation for $|\theta(101)|^2$. The mode $\theta(101)$ receives energy from the modes $\theta(\mathbf{p})$ and $\theta(\mathbf{q})$ of triads I: $\mathbf{k}' = (1,0,1)$; $\mathbf{p} = (0,1,1)$; $\mathbf{q} = (-1,-1,-2)$, II: $\mathbf{k}' = (1,0,1)$; $\mathbf{p} = (0,-1,1)$; $\mathbf{q} = (-1,1,-2)$, V: $\mathbf{k}' = (1,0,1)$; $\mathbf{p} = (-1,0,1)$; $\mathbf{q} = (0,0,-2)$. It also receives energy from interaction with the $u_3(101)$ mode. Hence

$$\begin{aligned}\frac{\partial}{\partial t}\frac{|\theta(101)|^2}{2} = {} & S_{\mathrm{I}}^{\theta\theta}(\mathbf{k}'|\mathbf{p}|\mathbf{q}) + S_{\mathrm{I}}^{\theta\theta}(\mathbf{k}'|\mathbf{q}|\mathbf{p}) + \Re\left[\theta(\mathbf{k})u_3^*(\mathbf{k})\right] \\ & + S_{\mathrm{II}}^{\theta\theta}(\mathbf{k}'|\mathbf{p}|\mathbf{q}) + S_{\mathrm{II}}^{\theta\theta}(\mathbf{k}'|\mathbf{q}|\mathbf{p}) \\ & + S_{\mathrm{V}}^{\theta\theta}(\mathbf{k}'|\mathbf{p}|\mathbf{q}) + S_{\mathrm{V}}^{\theta\theta}(\mathbf{k}'|\mathbf{q}|\mathbf{p}) \\ & - (\pi^2 + k^2)\theta(101).\end{aligned}$$

Using the mode-to-mode energy transfer formulas (eqs (8) and (9)) it is easy to show that

$$\begin{aligned} S_{\mathrm{I}}(\mathbf{k}'|\mathbf{p}|\mathbf{q}) &= S_{\mathrm{II}}(\mathbf{k}'|\mathbf{p}|\mathbf{q}) = \frac{\pi}{128}w_{101}\theta_{101}\theta_{112}, \\ S_{\mathrm{I}}(\mathbf{k}'|\mathbf{q}|\mathbf{p}) &= S_{\mathrm{II}}(\mathbf{k}'|\mathbf{q}|\mathbf{p}) = 0, \\ S_{\mathrm{V}}(\mathbf{k}'|\mathbf{p}|\mathbf{q}) &= 0, \\ S_{\mathrm{V}}(\mathbf{k}'|\mathbf{q}|\mathbf{p}) &= S_{\mathrm{V}}(\mathbf{k}'|\mathbf{q}|\mathbf{p}). \end{aligned}$$

Using these, we get the evolution equation for the Fourier mode θ_{101} as

$$\dot{\theta}_{101} = \frac{\pi}{4} w_{011}\theta_{112} + w_{101} + \pi w_{101}\theta_{002} - (\pi^2 + k^2)\theta_{101}. \tag{10}$$

Using similar analysis we derive the following evolution equations for the other Fourier modes:

$$\dot{\theta}_{011} = \frac{\pi}{4} w_{101}\theta_{112} + w_{011} + \pi w_{011}\theta_{002} - (\pi^2 + k^2)\theta_{011}, \tag{11}$$

$$\dot{\theta}_{112} = -\frac{\pi}{2}\left[w_{101}\theta_{011} + w_{011}\theta_{101}\right] + w_{112} - 2(2\pi^2 + k^2)\theta_{101}, \tag{12}$$

$$\dot{\theta}_{002} = -\frac{\pi}{2}\left[w_{101}\theta_{101} + w_{011}\theta_{011}\right] - 4\pi^2\theta_{002}, \tag{13}$$

$$\dot{w}_{101} = \frac{\pi}{4} w_{011}w_{112} + \frac{R * P * k^2}{\pi^2 + k^2}\theta_{101} - P(\pi^2 + k^2)w_{101}, \tag{14}$$

$$\dot{w}_{011} = \frac{\pi}{4} w_{101}w_{112} + \frac{R * P * k^2}{\pi^2 + k^2}\theta_{011} - P(\pi^2 + k^2)w_{011}, \tag{15}$$

$$\dot{w}_{112} = -\frac{\pi^2 + k^2}{2\pi^2 + k^2}\pi w_{101}w_{011} + \frac{R * P * k^2}{2\pi^2 + k^2}\theta_{112} - P * 2(2\pi^2 + k^2)w_{112}. \tag{16}$$

Note that eqs (10)–(16) contain two sets of Lorenz model [18] coupled with nonlinear modes w_{112} and θ_{112}. Since there are seven equations in the above model, we call it a seven-mode model. If we keep only $\theta_{002}, \theta_{101}, w_{101}$ (or $\theta_{002}, \theta_{011}, w_{011}$) modes, we obtain the famous Lorenz equations. Since two Lorenz equations are embedded in the above set, it is also called double-Lorenz model.

We have three free parameters (R, P, k) in the above set of equations. For the results presented in this paper, k is taken be its critical value (i.e., $k = k_c = \pi/\sqrt{2}$). Lorenz equation is not valid for small Prandtl number. In this paper we have taken $P = 10$. Note however that the qualitative features remain the same as long as $P > 1$.

We solve the above set of equations numerically by the given initial conditions. The results are described in the next section.

4. Results

The model (10)–(16) is solved numerically using fourth-order Runge–Kutta scheme. The parameters P and k are set to constant values of 10 and $\pi/\sqrt{2}$ respectively. We vary $r = R/R_c$, where $R_c = 27\pi^4/4$ is the critical Rayleigh number. As expected, all the variables are zero for $r < 1$. This region corresponds to conduction state.

Just above $r > 1$, we observe four different steady-state solutions:

(A1) $w_{011} = X_0;\ \theta_{011} = Y_0;\ \theta_{002} = Z_0,$
(A2) $w_{011} = -X_0;\ \theta_{011} = -Y_0;\ \theta_{002} = Z_0,$
(B1) $w_{101} = X_0;\ \theta_{101} = Y_0;\ \theta_{002} = Z_0,$
(B1) $w_{101} = -X_0;\ \theta_{101} = -Y_0;\ \theta_{002} = Z_0,$

where

$$X_0 = \frac{4}{3\pi}\sqrt{R - R_c}; \quad Y_0 = \frac{6\pi}{R}\sqrt{R - R_c}; \quad Z_0 = \frac{1}{\pi}\left(\frac{R_c}{R} - 1\right), \tag{17}$$

and the rest of the modes are zero. The above values are the fixed point values of Lorenz model, but with different normalization.

The pairs (A1), (A2) and (B1), (B2) are the Lorenz fixed points. Physically they are the stationary straight (i.e., 2D) rolls along the x and y directions respectively. As we will describe below, these two fixed points play a very important role in the dynamics. The choice of the solution depends on the initial condition; the initial conditions lying in the basin of attraction of the fixed points (A1, A2, B1, B2) approach the respective fixed points in the steady state.

The above rolls are steady-state solutions till $r \approx 14.3$. Near $r = 14.3$, the above-mentioned Lorenz fixed points become unstable, and a Hopf bifurcation takes place. In the state space we obtain limit cycles around the fixed points (A1), (A2) and (B1), (B2).

Let us focus on the fixed point (A2). When the fixed point is stable, θ_{011}, w_{011}, θ_{002} are constants, and the rest are zeros. After Hopf bifurcation, θ_{011}, w_{011}, θ_{002} oscillate around the fixed point values, and the other modes w_{101}, w_{112}, θ_{101}, θ_{112} start oscillating around zero as shown in figure 1. Hence two limit cycles are born; one of them is illustrated in figure 2 where we plot the projection of state space on the w_{101}–θ_{101} plane.

The physical interpretation of the above solution is quite interesting. Since the modes θ_{011}, w_{011}, θ_{002} are still dominant, there are strong rolls with axes along the x direction. The small and oscillatory values of w_{101} and θ_{101} indicate an emergence of rolls with axes along the y direction; these rolls appear and disappear. Hence, near the bifurcation around the fixed point (A2), we obtain asymmetric square pattern in the convection. These solutions were first obtained by Das *et al* [10].

Note that there are other stable limit cycle around the fixed points (A1), (B1), (B2). The state-space trajectories are attracted to one of the limit cycles depending on the initial conditions. The amplitudes of the limit cycle can be estimated in the following manner.

Let us consider Hopf bifurcation around the fixed point (A2). The mean values of the Fourier modes are

$$w_{011} = -\frac{4}{3\pi}\sqrt{R - R_c};\ \theta_{011} = -\frac{6\pi}{R}\sqrt{R - R_c};\ \theta_{011} = -\frac{6\pi}{R}\sqrt{R - R_c}$$

and the mean values of the other modes are zero. By keeping only the leading-order terms of eqs (10)–(16) we obtain

$$\dot{\theta}_{101} \approx \frac{\pi}{4} w_{011}\theta_{112},$$

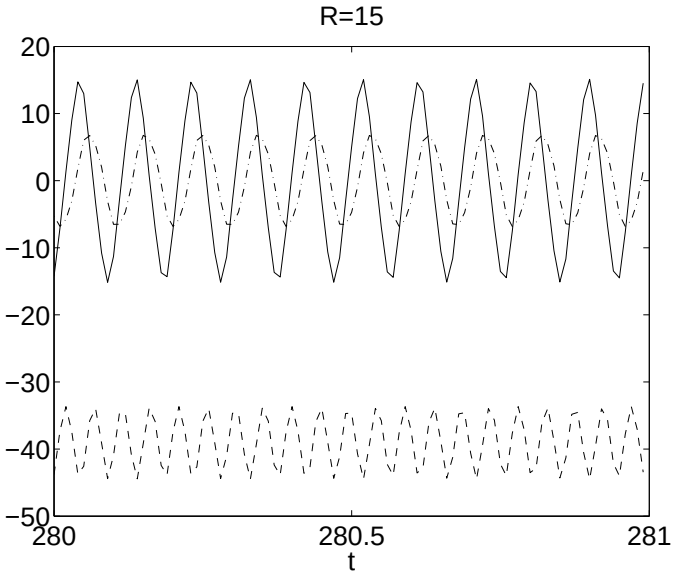

Figure 1. Time series plot of w_{101}, w_{011}, and w_{112} for $r = R/R_c = 15$, $P = 10$. W_{101} and W_{011} are represented by solid and dashed line with average around 0 and -40 respectively. W_{112} is the chained line oscillating around 0 with smaller amplitude.

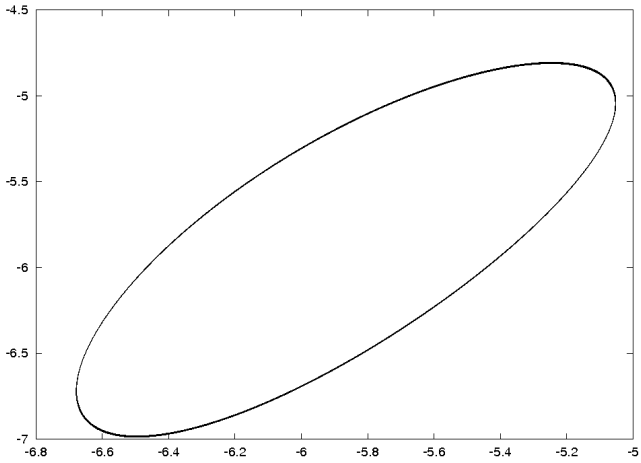

Figure 2. Projection of state space on w_{101}–θ_{101} plane for $r = R/R_c = 15$, $P = 10$. The trajectory is a limit cycle.

$$\dot{\theta}_{112} \approx -\frac{\pi}{2} w_{011}\theta_{101},$$
$$\dot{w}_{101} \approx \frac{\pi}{4} w_{011}w_{112},$$

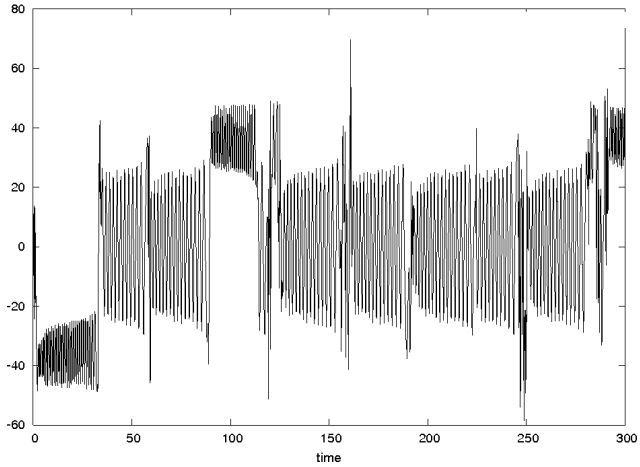

Figure 3. Plot of $w_{101}(t)$ vs. t for $r = R/R_c = 15.22$, $P = 10$. The system oscillates around a fixed point in a quasi-periodic manner, then it jumps to the other fixed point abruptly. The trajectory is chaotic.

$$\dot{w}_{112} \approx -\frac{3\pi}{5} w_{011} w_{101}.$$

The solution of the above equations imply that θ_{101} and θ_{112} oscillate with frequency $\pi w_{011}/(2\sqrt{2})$, while w_{101} and w_{112} oscillate with frequency $\pi w_{011}\sqrt{3/20}$. The analytical solution also indicates that 101 and 112 modes have a phase difference of $\pi/2$. The frequencies from our numerical simulation of eqs (10)–(16) match quite well with the above estimates. However, the phases are quite different from $\pi/2$. The difference is due to the neglect of other terms. Thus this simple analysis gives the frequency of Hopf bifurcation quite well. Note that the bifurcation around other fixed points have has identical nature.

When we increase r further, we obtain limit cycle up to $r = 15.22$. At $r = 15.22$ the state-space trajectories are not closed. We find that a point moves around a fixed point, and then it jumps toward the other fixed point, and it revolves around that. Then it again comes back to the first fixed point. This behaviour is illustrated in the time series plot shown in figure 3, and it is reminiscent of Lorenz equation. The time series shows a large region of regular behaviour (oscillations around the fixed points), and a small region of turbulent behaviour (jumps). These properties are signatures of emergence of chaos by intermittency route.

The time series plot indicates another important behaviour. We observe that sometimes w_{101} oscillates around a mean value, and sometimes it oscillates around zero. These two cases are complementary asymmetric square patterns (A,B, i.e., strong rolls along y and x directions respectively). Hence, the system switches from a configuration of asymmetric square to the other configuration. Figure 4 shows the projection of the state space on the w_{101}–θ_{101} plane, which again indicates a chaotic behaviour. The largest Lyapunov exponent is approximately 0.047.

The power spectrum of the signal w_{101} is shown in figure 5. This spectrum shows one dominant frequency with a small broadening near it. The peak in the power

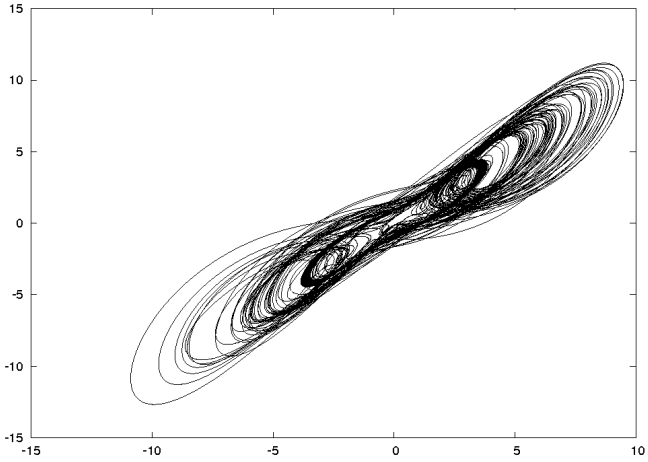

Figure 4. Projection of state space on w_{101}–θ_{101} plane for $r = R/R_c = 15.22$, $P = 10$. The trajectory is chaotic.

spectrum corresponds to the oscillations around the fixed points, and the power in the other frequencies corresponds to the jumps from one fixed point to the other. Note that period-doubling route to chaos exhibit peaks at subharmonics ($f/2, f/4$ etc.), and quasi-periodic route to chaos also exhibits peaks in the power spectrum at different frequencies (e.g., sum and differences of two dominant frequencies) [19]. Due to these reasons, emergence of chaos by period-doubling and quasi-periodic is ruled out for the 7-mode model presented in our paper.

When we increase r beyond 15.22, the laminar region keeps shrinking. For r near 30, we do not observe any laminar region, and the state space is completely chaotic. Since, these features are known very well in the literature, we are not presenting details for r beyond 15.22. The results presented here are in agreement with earlier numerical results of Das *et al* [10].

5. Conclusions

We have presented in this paper a novel method for using mode-to-mode energy transfer to investigate interacting dissipative structures in a model of thermal convection. The dynamical system presented here provides a *toy* model to investigate chaotic dynamics of competing patterns in thermal convection. In addition, we have presented an analytical model for the limit cycle which emerges in the system.

In the present paper we have provided an analytic argument for the emergence of competing asymmetric square pattern in convection. Our theoretical reasoning provide justification for the asymmetric square patterns observed experimentally by Assenheimer and Steinberg [16], and numerically by Busse and Clever [11] and Sanchez-Alvarez *et al* [17]. These arguments are in continuation of those provided by Das *et al* [10].

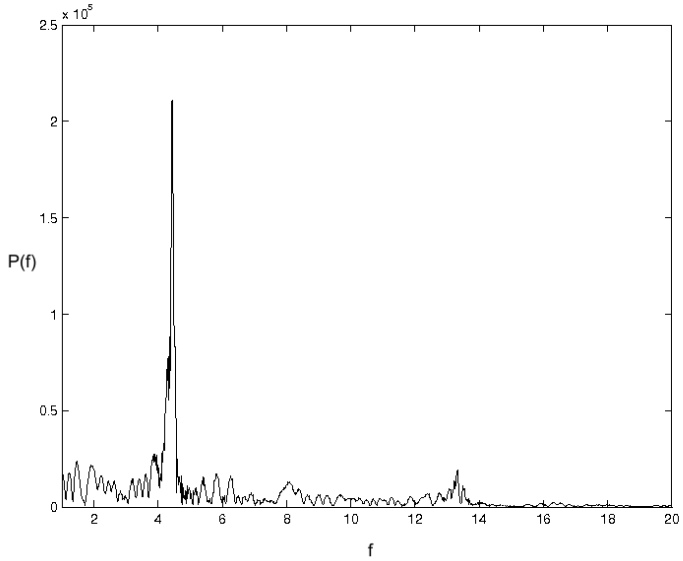

Figure 5. Power spectrum of the signal w_{101} for $r = R/R_c = 15.22$, $P = 10$. The spectrum shows a narrow band of frequencies around the dominant frequency.

The energy transfers among Fourier modes could provide interesting insights into dynamics of various patterns observed in convective flows. We are in the process of studying convective systems like zero-Prandtl number flows, dynamo model etc. in this light.

References

[1] G K Batchelor, *J. Fluid Mech.* **5**, 113 (1959)
[2] G Dar, M K Verma and V Eswaran, *Physica* **D157**, 207 (2001)
[3] F Bataille, Y Zhou and J P Bertoglio, ICASE Rep. No. 97-62 (NASA CR-97-206249) (1997)
[4] G K Batchelor, I D Howells and A A Townsend, *J. Fluid Mech.* **5**, 134 (1959)
[5] R Kraichnan, *Phys. Fluids* **11**, 945 (1968)
[6] R H Kraichnan, *J. Fluid Mech.* **5**, 497 (1959)
[7] M Lesieur, *Turbulence in fluids – Stochastic and numerical modelling* (Kluwer Academic Publishers, Dordrecht, 1990)
[8] K Ohkitani and S Kida, *Phys. Fluids* **A4**, 794 (1992)
[9] M K Verma, *Phys. Rep.* **401**, 229 (2004)
[10] A Das, U Ghosal and K Kumar, *Phys. Rev.* **62**, 3051 (2000)
[11] F H Busse and R M Clever, *Phys. Rev. Lett.* **81**, 341 (1998)
[12] H W Müller and M Lücke, *Phys. Rev.* **A38**, 2965 (1988)
[13] K Kumar, *Phys. Rev.* **A41**, 3134 (1990)
[14] A Schlüter, D Lortz and F H Busse, *J. Fluid Mech.* **32**, 129 (1965)
[15] J A Whitehead and B Parson, *Geophys. Astrophys. Fluid Dyn.* **9**, 201 (1978)
[16] M Assenheimer and V Steinberg, *Phys. Rev. Lett.* **76**, 756 (1996)

[17] J J Sanchez-Alvarez, E Serre, E C delArco and F H Busse, *Phys. Rev.* **E72**, 036307 (2005)
[18] E N Lorenz, *J. Atmos. Sci.* **20**, 130 (1963)
[19] R C Hilborn, *Chaos and nonlinear dynamics* 2nd edition (Oxford University Press, Oxford, 2000)